2016

Effect of Channel Geometries on Flow Reversal in Microchannel Evaporators

Huize Li
University of Illinois at Urbana-Champaign, United States of America, huizeli2@illinois.edu

Pega Hrnjak
University of Illinois at Urbana-Champaign, United States of America, pega@illinois.edu

Effect of channel geometries on flow reversal in microchannel evaporators

Huize LI[1], Pega HRNJAK[1,2]*

[1]University of Illinois at Urbana-Champaign, Mechanical Science and Engineering, Urbana, IL, USA
huizeli2@illinois.edu, pega@illinois.edu

[2]CTS, Creative Thermal Solutions, Urbana, IL, USA

* Corresponding Author

ABSTRACT

Flash Gas Bypass with venting of reversed vapor is implemented in a R134a automotive air conditioning system. The mass flow rate of reversed vapor is measured by a flow meter placed on the venting line. The effects of microchannel geometries including channel length and channel diameter on the amount and frequency of flow reversal are investigated. A mechanistic model is developed to simulate the bubble dynamics inside of single microchannel tube. This model is validated against experimental data and used to explain the effect of channel length and diameter on flow reversal.

1. INTRODUCTION

Microchannel heat exchangers are widely used in air conditioning and refrigeration systems because of their compactness and enhancement of heat transfer performance. However microchannel heat exchangers suffer from the problem of refrigerant maldistribution, especially for evaporator. For condensers, refrigerant distribution has less effect on performance, on the other hand, better separation of flow might be desired instead of better mixing (Li and Hrnjak, 2016). The none-uniform distribution of two phase refrigerant in evaporator can significantly deteriorate the evaporator performance as well as system efficiency. Boiling instability and flow reversal is one cause for refrigerant maldistribution. According to Tuo and Hrnjak (2013a), flow reversal in microchannel evaporators deteriorates refrigerant distribution, increase pressure drop, although may increase local heat transfer coefficient. The focus of previous research on flow instability in microchannels has been on heat sinks for small scale cooling applications, such as electronic cooling. Brutin et al. (2003) experimentally investigated the unsteady boiling of n-Pentane in heated minichannels. They found that the unsteady boiling region was determined by heat flux and mass velocity, and unsteady boiling created reverse flow and high amplitude fluctuation of pressure signal. Brutin and Tadrist (2004) further studied the steady and unsteady boiling region determined by heat flux and mass velocity. They found that under each heat flux they examined, there is a critical mass velocity (or Re number) that delimit steady and unsteady boiling. Under each heat flux, unsteady boiling only happens at low mass velocity region, which can also be interpreted as high exit quality region. They also examined both confined inlet and compliant inlet (with a buffer) and discovered that pressure drop oscillation has lower amplitude but higher frequency in compliant inlet case compared with confined inlet case. Wu and Cheng (2003) studied water boiling in two silicon microchannels with diameters of 158.8 and 82.8 micron. They believed a new type of oscillation with long period was discovered in which single phase flow and two-phase flow appear alternatively. The oscillation period in the large channel was 31 s, and it was 141 s in the smaller tube. Wu and Cheng (2004) continued their study about boiling instability in parallel microchannels. They first adjusted the water inlet pressure, then gradually increased heat flux. They discovered liquid/two-phase alternating flow at heat flux from 13.5-16.6 W/cm^2, then continuous two-phase flow at heat flux of 18.8 W/cm^2, and lastly liquid/two-phase/vapor alternating flow at heat flux of 22.6 W/cm^2. They found that liquid/two-phase/vapor alternating flow created the largest pressure oscillation, while continuous two-phase generated the least pressure oscillation. Wu and Mudawar (2004) studied boiling instability of water in parallel microchannels under high heat fluxes. They were focusing on two types of dynamic instability:

pressure drop oscillation and parallel channel instability. They found that pressure drop oscillation can be greatly suppressed by a throttling valve placed before microchannels. Parallel channel instability, which is much milder than pressure oscillation, can also be alleviated by more throttling. They also discovered that under the same mass flux, higher heat flux will help to stabilize the boiling process because the system becomes stiffer with increasing pressure drop and a smaller portion of two-phase flow. Hestroni et al., (2005) proposed detailed stages in one cycle of periodic boiling process. Soon after nucleation, a bubble grows very rapidly to the size comparable to the diameter of the channel (step a); then the bubble expands bidirectionally (step b); after the downstream edge of the bubble reaches channel outlet, the bubble begins to vent (step c); few liquid droplets are left on the wall after bubble depletion (step d); along with bubble depletion, pressure inside of the channel decreases and fresh liquid starts to move in (step e); finally, a new cycle starts (step f). Through experiments, they also found that pressure oscillation caused by boiling instability increases with increasing quality. Hetroni et al., (2006) tried to describe boiling instability by dimensionless groups. They picked Nusselt number (Nu), Eotvos number (Eo) and Boiling number (Bo). They correlated initial film thickness and Nu/Eo with Bo and believed Bo (q/mh_{fg}) is the bond between momentum and energy equations. Chen and Garimella (2006) visualized FC-77 flow in parallel silicon microchannels. They found that under high heat fluxes (>427 kW/m^2), flow reversal occurs near the inlet of the microchannels, causing oscillation of pressure drop. They also concluded that flow reversal, which creates changes of mass flow rate, causes the alternation of flow regime near the outlet of the microchannel. From their results, it can be seen that higher heat flux leads to greater chance of reverse flow, but this comparison is made under the same mass flux and changing outlet quality (under same mass flux, higher heat flux will create higher exit quality). Harirchian and Garimela (2008) visualized FC-77 flow in parallel silicon microchannels with different geometries. They located a throttling valve before the heat sink to suppress instability, but flow reversal was still observed at their highest heat flux examined. Huh et al. (2007) studied boiling instability in one microchannel. They discovered that there is a phase shift between pressure drop oscillation and mass flow oscillation. A sudden increase of mass flow rate occurred at the peak of pressure drop. They also found that an increase of mass flow rate lead to smaller oscillation amplitude and shorter period. Under the same mass flux, increasing heat flux (equivalent to higher exit quality) created higher oscillation amplitude and longer period. Zhang et al. (2009) investigated excursive instability in parallel microchannels. They found that increasing operation pressure, channel diameter, and channel length and adding an inlet restrictor could alleviate instability.

The heat transfer and fluid flow conditions in heat sinks for electronic cooling are significantly different from those in air conditioning systems. In heat sinks, the incoming flow is normally subcooled and the exit quality is very low, while in microchannel evaporators of A/C systems, the fluid at the inlet is either two-phase or saturated liquid and the outlet is normally superheated. In addition, the heat flux in electronic cooling applications is much higher than that in air conditioning applications. Last but not least, water is the most commonly used fluid in the reviewed studies, and its thermophysical properties (vapor density, heat of vaporization, etc.) are significantly different with those of hydrofluorocarbons (R134a, R410A, etc.). To the best of the authors' knowledge, the flow reversal in real systems was first observed at CTS (Creative Thermal Solutions) in 2006 and later published by Bowers et al (2012). The only studies of flow reversal and boiling instability in realistic air conditioning systems in open literature were carried out by Tuo and Hrnjak. They (2013b) invented a new system configuration to vent the reversed vapor in the evaporator. They found that the reverse vapor accounted for 2-8% of the total supplied liquid into the evaporator. By venting the reverse vapor, 5 % of capacity and 3 % of COP improvement could be achieved compared with the flash gas removal (FGB) AC system baseline. The Flash Gas Bypass system was first used for systems with microchannel evaporators by Beaver, Hrnjak (2000), later Elbel and Hrnjak (2004).

The focus of this research is to experimentally investigate boiling instability and flow reversal in microchannel evaporators under conditions and geometries which are relevant to air conditioning applications. Meanwhile, a mechanistic model of bubble dynamics in microchannels will be developed and validated using experimental results. This model will be used to explain the effect of different geometries on flow reversal.

2. EXPERIMENTAL SETUP AND TEST CONDITIONS

The schematic drawing of the facility is shown in Figure 1**Error! Reference source not found.**. The variable speed compressor and the microchannel condenser are components that are used in a major brand vehicle. Three different microchannel evaporators were examined in the system with detailed geometry summarized in Table 1. Two heat exchangers have identical channel length but with different channel diameter, and another two share the same

microchannel tube cross-section but with different length. The cross-sections of two microchannel tubes are shown in Figure 2.

In order to measure the flow rate of reversed vapor, revised flash gas bypass (FGBR) configuration invented by Tuo and Hrnjak (2013b) is employed (as shown in Figure 3), which is a modification of Flash Gas Bypass (FGB) configuration. In FGB mode, a separation vessel is placed before the evaporator, ensuring that only liquid is supplied to the evaporator and vapor is bypassed to the inlet of a compressor. Based on FGB configuration, two venting ports are added near both ends of the inlet header in FGBR mode, directing the reversed vapor to the top of the separation vessel. The dynamic mass flow rate of reversed vapor is measured by a mass flow meter, which is placed on the venting line.

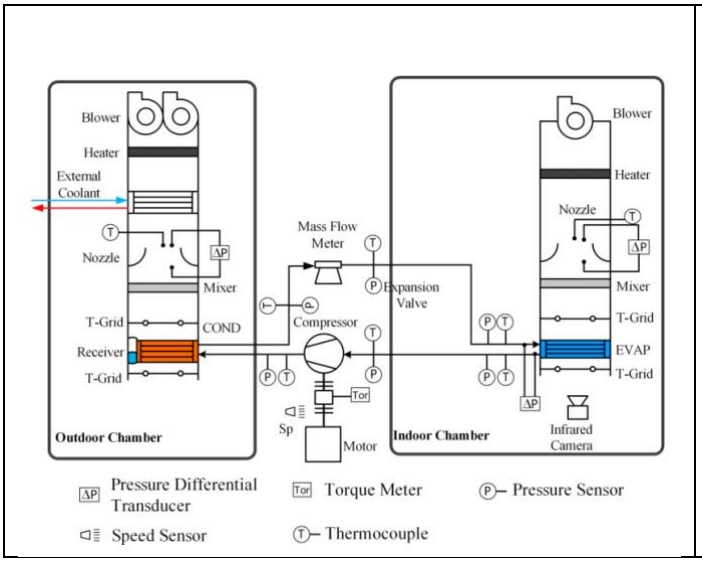

Figure 1. Schematic drawing of the test facility

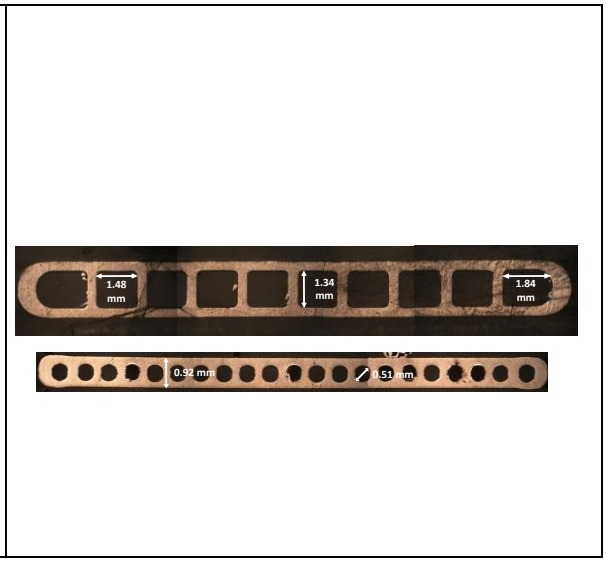

Figure 2. Cross-section of two types of MC examined

Table 1. Key geometries and operating conditions of three different heat exchangers (HX)

	Hydraulic diameter (mm)	Number of tubes	Channels /tube	Length (mm)	Refrigerant-side area /channel (mm^2)	Heat flux (kW/m^2)	Superheat (℃)
HX 1	1.4	25	10	190.0	1099.9	8.3-12.2	3.0-7.7
HX 2	0.5	35	21	190.0	304.4	7.3-16.3	1.9-7.5
HX 3	0.5	35	21	510.0	817.1	4.7-6.6	2.4-5.0

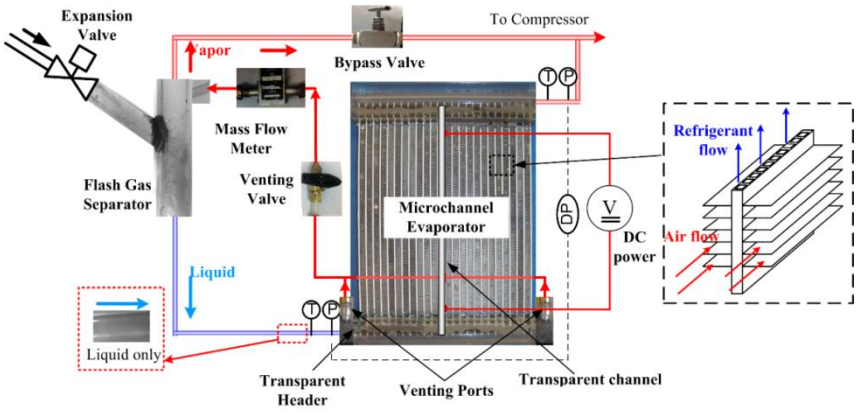

Figure 3. Evaporator setup in FGBR mode

3. RESULTS AND DISCUSSION

3.1 Model Development and Validation

The details of the model can be found in Li and Hrnjak (2016). The velocity and acceleration of each liquid slug is determined by the pressure in the bubbles located upstream and downstream:

$$P_{i-1,d}A - P_{i,u}A + F_{fric,l,i} + m_{l,i}g = m_{l,i}\frac{dV_i}{dt} \tag{3.1}$$

At the same time, the velocity difference of two neighboring liquid slugs is determined by the mass and energy balance of the bubble which is sandwiched in between.

$$\frac{dm_{v,i}}{dt}h_{lv} = \dot{q}\pi D(L_{v,i} + \frac{L_{l,i}}{2} + \frac{L_{l,i+1}}{2}) \tag{3.2}$$

$$\frac{dm_{v,i}}{dt} = \rho_v A\frac{dL_{v,i}}{dt} \tag{3.3}$$

The increase of the bubble length is caused by the velocity difference on both ends and the decrease in length of the liquid slug located upstream and downstream. In the end, the velocity difference of two neighboring liquid slugs is formulated (equation 3.5) as a function of heat flux, densities, heat of vaporization, lengths of liquid and vapor slugs and channel diameter.

$$\frac{dL_{v,i}}{dt} = V_{i+1} - V_i + \dot{q}\pi D(\frac{L_{l,i}}{2} + \frac{L_{v,i}}{2})/\rho_l Ah_{lv} + \dot{q}\pi D(\frac{L_{l,i+1}}{2} + \frac{L_{v,i}}{2})/\rho_l Ah_{lv} \tag{3.4}$$

$$V_{i+1} - V_i = \frac{\dot{q}\pi D(L_{v,i} + \frac{L_{l,i}}{2} + \frac{L_{l,i+1}}{2})(1-\frac{\rho_v}{\rho_l})}{\rho_v Ah_{lv}} = \frac{4\dot{q}(L_{v,i} + \frac{L_{l,i}}{2} + \frac{L_{l,i+1}}{2})(1-\frac{\rho_v}{\rho_l})}{\rho_v Dh_{lv}} \tag{3.5}$$

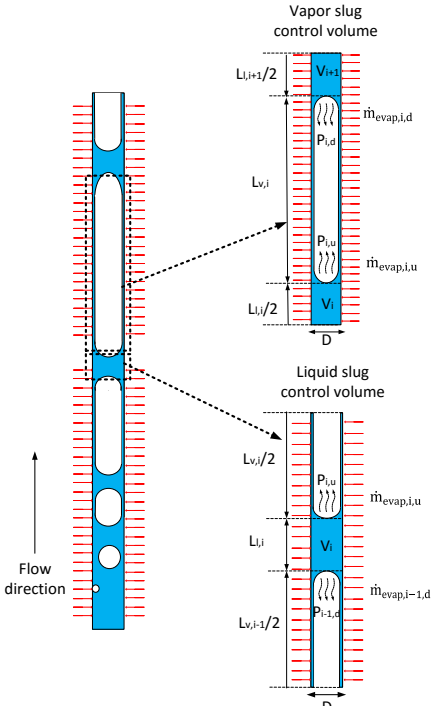

Figure 4. Control volumes for liquid and vapor slugs

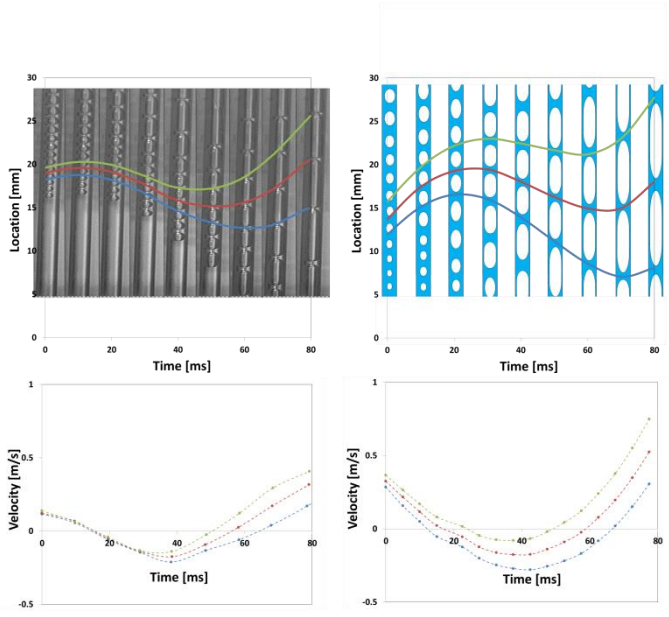

Figure 5. Comparison between flow visualization and simulation results

Knowing the pressures at the channel inlet and outlet (boundary conditions) and the velocity difference of any two neighboring liquid slugs, the pressure at each vapor slug (pressure will be different at the leading and trailing edges of the bubble, if vapor pressure drop is considered) and the velocity of each liquid slug can be calculated iteratively. The simulation results are compared with visualization results (Tuo and Hrnjak 2014) at the same geometry and similar operating conditions as shown in Table 2. Pressure drop in the model was modified to be 3 kPa to better match with the flow visualization results.

Table 2. Experimental conditions which are used as model inputs

Items	Unit	Value
Evaporation pressure	kPa	325
Heat flux	kW/m^2	8
Pressure drop	kPa	1.3

The top row in Figure 5 shows the comparison of bubble movement in experiment and simulation. The locations of three selected liquid slugs are highlighted using green, red and blue lines. The top left figure consists of 9 snapshots taken from the high speed video of the diabatic in-tube flow. The top right figure is generated using the numerical values of the locations of bubbles and liquid slugs at different points in time. It can be seen that the model is able to capture the experimental phenomenon of "forward flow-reverse flow-forward flow". The bottom row in Figure 5 shows the comparison of bubble velocity in experiment and simulation. The velocities in the experiment are calculated using the traveling distance of a certain liquid slug divided by the corresponding time interval. The bottom right figure is generated using the numerical values of the velocities of bubbles and liquid slugs at different points in time. The model is able to predict that the three liquid slugs begin to reverse around 20ms, and the velocity of the top liquid slug (green line) increases back to a positive value around 50ms followed by the next two liquid slugs. The bubble velocities of all three slugs seem to be the same before 15ms in the experiment. This is most likely because the majority of the heat input is used to superheat the new coming liquid refrigerant, but this factor is not considered in the model.

3.2 Effect of Channel Diameter

In this study, HX1 and HX2 are chosen since they have the same channel length (190 mm) but different channel diameter (1.4 mm and 0.5 mm). Similar operation conditions are imposed for both heat exchangers (around 7.8 kW/m^2 heat flux and 7.5℃ superheat). As shown in Figure 6(a), the mass flow rate of vented vapor (for whole heat exchanger) has a very obvious periodic oscillation in HX1, which is in phase with the oscillation of inlet and outlet pressures. Through Fast Fourier Transformation (FFT) of the temporal data, the dominant frequency is found to be 0.73 Hz. In HX2 (shown in Figure 6(b)), the frequency of oscillation increases to 1.05 Hz, but the amplitude significantly reduces. The ratio of vented vapor flow rate to the total mass flow rate is much higher in HX2 (14.8%) than in HX1 (6.6%).

Bubble dynamics in these two channels are simulated under the same operation conditions as in the experiments. The simulation and experimental results are summarized in Table 3. Although simulation results are not quantitatively similar with experimental results, but they shows the same trends with the experiments: There is more flow reversal being generated in the channel with 0.5mm diameter in terms of relative magnitude (vented vapor flow rate divided by the total mass flow rate supplied to the evaporator) with a higher frequency.

Table 3. Key flow reversal related measurements and simulation results in HX1 and HX2

Items	Mass flux in channels (kg/m^2)		Ratio[(a)]		Frequency (Hz)	
	Experiment	Simulation	Experiment	Simulation	Experiment	Simulation
HX 1	22.3	29.8	6.6%	0.9%	0.80	2.6
HX 2	50.2	54.9	14.6%	5.3%	1.05	4.1

(a): Ratio is defined as: vented vapor flow rate divided by the total mass flow rate supplied to the evaporator ($\dot{m}_{rev} / \dot{m}_{tot}$)

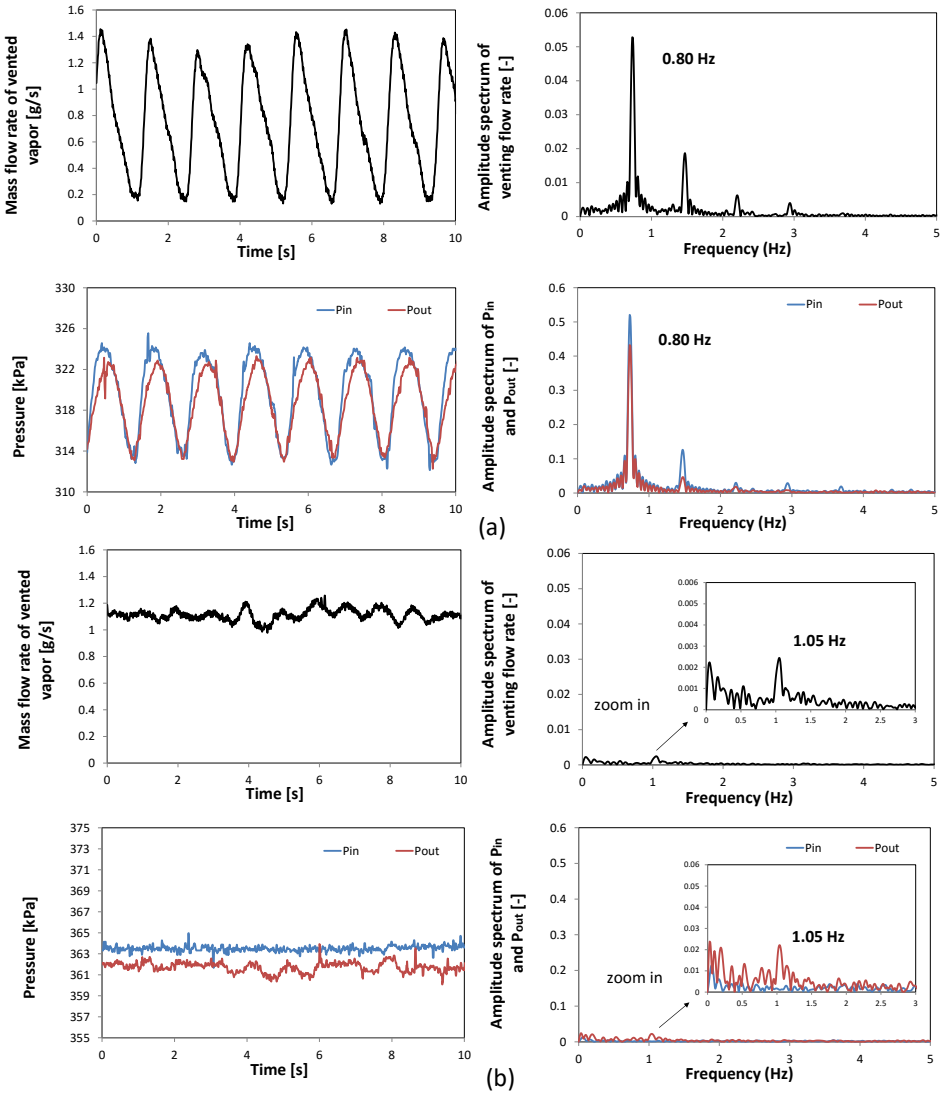

Figure 6. Temporal variations and frequency analyses of measured variables in HX 1 and HX 2

Refer to equation 3.5, under the same heat flux, smaller channel diameter will lead to more rapid growth of a bubble. There are larger differences of the velocities of the liquid slugs which are located upstream and downstream of the bubble. Frictional resistance created by liquid or vapor slugs is proportional to velocity squared. Due to a more drastic increase of liquid slug velocity in smaller channels, the frictional resistance is more concentrated downstream in the tube. Due to higher frictional resistance downstream, flow in smaller channels tends to decelerate quicker and the pressure peak will shift more downstream from the inlet. Figure 7 and 8 show the simulated flow regime and the corresponding pressure distribution inside of channels with 1.4 mm and 0.5 mm diameter, respectively. One periodic cycle is divided into 10 steps to demonstrate the evolution of flow regime and pressure distribution. For the large tube (1.4 mm), the highest pressure (indicated by the darkest red) occurs at 78% of the cycle time and is located very close to the tube inlet, creating small amount of flow reversal, which is confirmed by the flow regime shown on the left side of Figure 7. In the figures of flow regime, the black and white areas indicate liquid and vapor. Dash lines were used to illustrate the locations of the chosen liquid slugs in time. In the channel with smaller diameter (0.5mm), highest pressure occurs at 67% of the cycle time and is observed near 20 % of the tube length after the inlet, creating a negative pressure gradient in the first 20 % of the tube. Due to the negative pressure gradient which occurs earlier and covers more areas, there is more reverse flow in the channel with 0.5mm diameter, and this phenomenon is also demonstrated by the flow regime shown on the left side of Figure 8.

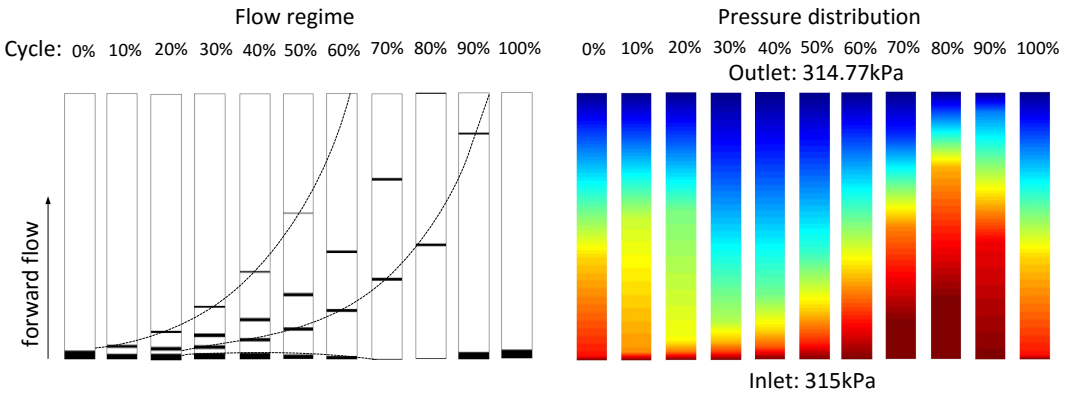

Figure 7. Flow regime and pressure distribution of R134a inside of a microchannel with 1.4 mm diameter and 190 mm length at 10 different points in time within one periodic cycle

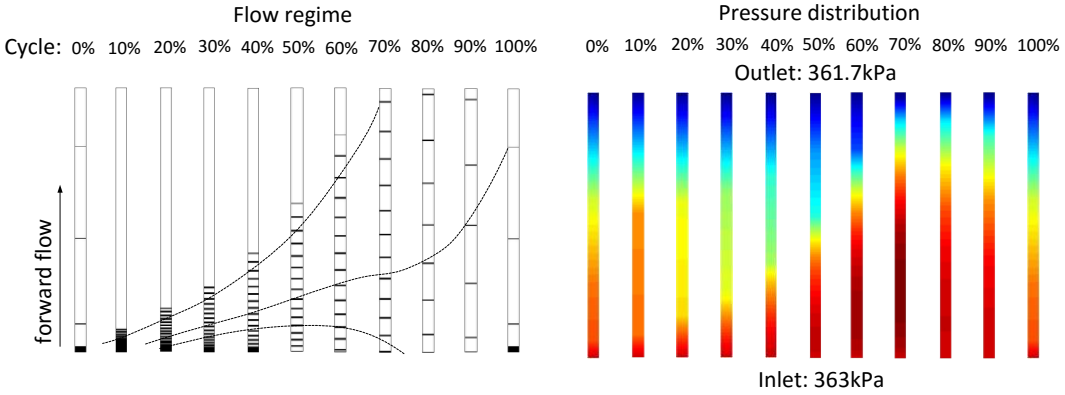

Figure 8. Flow regime and pressure distribution of R134a inside of a microchannel with 0.5 mm diameter and 190 mm length at 10 different points in time within one periodic cycle

3.3 Effect of Channel Length

In this study, HX2 and HX3 were chosen since they have the same channel diameter (0.5 mm) but different channel length (190 mm and 510 mm). Similar operation conditions are imposed for both heat exchangers (around 6.8 kW/m^2 heat flux and 6.5℃ superheat). By comparing Figure 6(b) and Figure 9, it can be seen that the oscillation amplitude of vented vapor flow is higher in HX3 than in HX2, but the frequency is lower in HX3 than in HX2. Larger oscillation is due to the fact that longer tube contains more refrigerant mass and more vapor will be vented within one periodic cycle. At the same time, more inertia associated with more refrigerant mass will slow down the periodic process, which contributes to slower frequency. Although the mass flux in HX3 is 1.5 times higher than that in HX2, the ratio of vented vapor flow rate to the total mass flow rate supplied to the evaporator in HX3 (10.1%) is only slightly lower than that in HX2 (14.6%),

Bubble dynamics in these two channels are simulated under the same operation conditions as in the experiments. The simulation and experimental results are summarized in Table 4. Although simulation results are not quantitatively similar with experimental results, but they shows the same trends with the experiments: There is slightly more flow reversal being generated in the channel with 190mm length in terms of relative magnitude (vented vapor flow rate divided by the total mass flow rate supplied to the evaporator) with a slightly higher frequency. For the channel with 510 mm length, the simulated flow regime and pressure distribution at 10 selected times within one cycle are presented in Figure 10. The location of the highest pressure is also close to 20% of the tube length after the inlet and it occurs at 68.6% of the cycle time, which is similar with the case in 190 mm tube. Despite the large difference of mass flux in both channels, the relative magnitude of vented vapor flow rate in both channels differs not significantly (shown by both experiments and simulation), and this can be attributed to the similar pressure distribution along two channels.

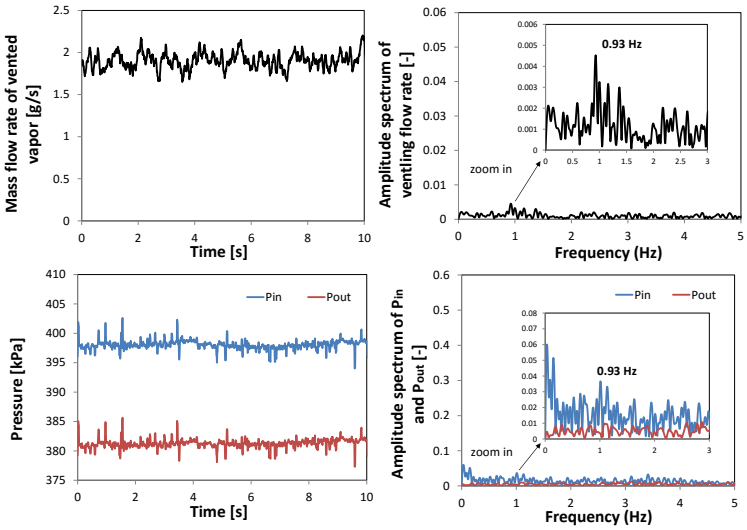

Figure 9. Temporal variations and frequency analyses of measured variables in HX 3

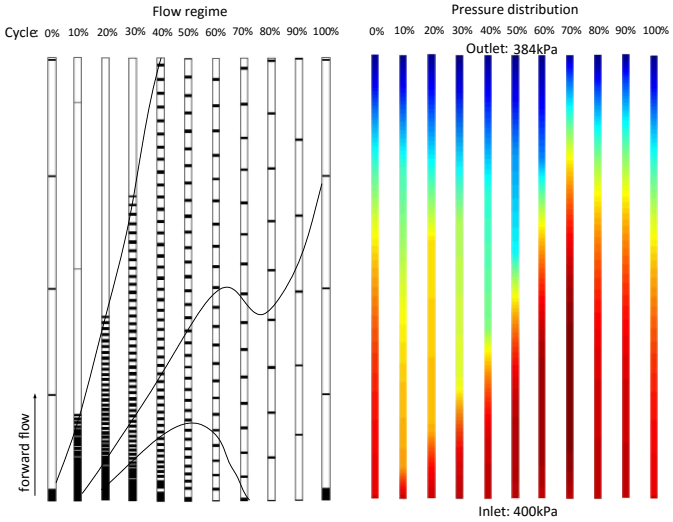

Figure 10. Flow regime and pressure distribution of R134a inside of a microchannel with 0.5 mm diameter and 510 mm length at 10 different times within one periodic cycle

Table 4. Key flow reversal related measurements and simulation results in HX2 and HX3

Items	Mass flux in channels (kg/m^2)		Ratio		Frequency (Hz)	
	Experiment	Simulation	Experiment	Simulation	Experiment	Simulation
HX 2	50.2	54.9	14.6%	5.3%	1.05	4.1
HX 3	127.1	151.2	10.1%	4.9%	0.93	3.7

4. CONCLUSION

It has been found experimentally that under the same heat flux (based on the refrigerant side area), microchannel evaporators with same length but smaller diameter induce more reverse flow ($\dot{m}_{rev}/\dot{m}_{tot}$) at a higher frequency, and microchannel evaporators with same diameter but longer length produce slightly less reverse flow ($\dot{m}_{rev}/\dot{m}_{tot}$)

at a slightly slower frequency. The effect of diameter on flow reversal (relative mass flow rate ratio and frequency) is more significant than the effect of channel length.

A newly developed mechanistic model which can simulate bubble dynamics in single microchannel explains the experimental results: under the same heat flux and smaller diameter, the vapor slug grows more rapidly (according to equation 3.5), locating more flow resistance to the downstream part of a channel. The higher downstream resistance will decelerate the incoming flow quicker and generate negative pressure gradient in larger upstream areas, which leads to more flow reversal at higher frequency. For microchannel evaporators with same diameter but different length, the pressure distribution along channel length is rather similar. Slightly more flow reversal ($\dot{m}_{rev} / \dot{m}_{tot}$) at a higher frequency in shorter heat exchangers is attributed to less incoming mass flux.

NOMENCLATURE

A	area	(m^2)
D	diameter	(D)
F	force	(N)
g	acceleration of gravity	(m^2/s)
h	enthalpy	(kJ/kg)
L	length	(m)
m	mass	(kg)
ρ	density	(kg/m^3)
P	pressure	(kPa)
$\dot{q}$	heat flux	(kW/m^2)
t	time	(s)
V	velocity	(m/s)
Subscript		
evap	evaporation	
d	downstream	
i	index	
l	liquid	
rev	reversed vapor	
tot	total supplied liquid	
u	upstream	
v	vapor	

REFERENCES

Brutin, D., Topin, F., & Tadrist, L. (2003). Experimental study of unsteady convective boiling in heated minichannels. International Journal of Heat and Mass Transfer, 46(16), 2957–2965. doi:10.1016/S0017-9310(03)00093-0

Brutin, D., & Tadrist, L. (2004). Pressure drop and heat transfer analysis of flow boiling in a minichannel: Influence of the inlet condition on two-phase flow stability. International Journal of Heat and Mass Transfer, 47(10-11), 2365–2377. doi:10.1016/j.ijheatmasstransfer.2003.11.007

Wu, H. Y., & Cheng, P. (2003). Visualization and measurements of periodic boiling in silicon microchannels. International Journal of Heat and Mass Transfer, 46(14), 2603–2614. doi:10.1016/S0017-9310(03)00039-5

Wu, H. Y., & Cheng, P. (2004). Boiling instability in parallel silicon microchannels at different heat flux. International Journal of Heat and Mass Transfer, 47(17-18), 3631–3641. doi:10.1016/j.ijheatmasstransfer.2004.04.012

Hestroni, G., Mosyak, A., Pogrebnyak, E., & Segal, Z. (2005). Explosive boiling of water in parallel micro-channels. International Journal of Multiphase Flow, 31(4), 371–392. doi:10.1016/j.ijmultiphaseflow.2005.01.003

Hestroni, G., Mosyak, A., Pogrebnyak, E., & Segal, Z. (2006). Periodic boiling in parallel micro-channels at low vapor quality. International Journal of Multiphase Flow, 32(10-11), 1141–1159. doi:10.1016/j.ijmultiphaseflow.2006.06.005

Chen, T., & Garimella, S. V. (2006). Measurements and high-speed visualizations of flow boiling of a dielectric fluid in a silicon microchannel heat sink. International Journal of Multiphase Flow, 32(8), 957–971. doi:10.1016/j.ijmultiphaseflow.2006.03.002

Harirchian, T., & Garimella, S. V. (2008). Microchannel size effects on local flow boiling heat transfer to a dielectric fluid. International Journal of Heat and Mass Transfer, 51(15-16), 3724–3735. doi:10.1016/j.ijheatmasstransfer.2008.03.013

Huh, C., Kim, J., & Kim, M. H. (2007). Flow pattern transition instability during flow boiling in a single microchannel. International Journal of Heat and Mass Transfer, 50(5-6), 1049–1060. doi:10.1016/j.ijheatmasstransfer.2006.07.027

Zhang, T., Tong, T., Chang, J. Y., Peles, Y., Prasher, R., Jensen, M. K., … Phelan, P. (2009). Ledinegg instability in microchannels. International Journal of Heat and Mass Transfer, 52(25-26), 5661–5674. doi:10.1016/j.ijheatmasstransfer.2009.09.008

Tuo, H., & Hrnjak, P. (2013a). Periodical reverse flow and boiling fluctuations in a microchannel evaporator of an air-conditioning system. International Journal of Refrigeration, 36(4), 1263–1275. doi:10.1016/j.ijrefrig.2013.02.001

Tuo, H., & Hrnjak, P. (2013b). New approach to improve performance by venting periodic reverse vapor flow in microchannel evaporator. International Journal of Refrigeration, 36(8), 2187–2195. doi:10.1016/j.ijrefrig.2013.05.020

Tuo, H., & Hrnjak, P. (2014). Visualization and measurement of periodic reverse flow and boiling fluctuations in a microchannel evaporator of an air-conditioning system. International Journal of Heat and Mass Transfer, 71, 639–652. doi:10.1016/j.ijheatmasstransfer.2013.10.024

Li, H. and Hrnjak, P., "Visualization and Analysis of Periodic Reverse Flow in an Automobile Microchannel Evaporator," SAE Technical Paper 2016-01-0252, 2016, doi:10.4271/2016-01-0252.

Beaver, A. C., J. M Yin, C. W. Bullard, and P. S. Hrnjak, An Experimental Investigation of Transcritical Carbon Dioxide Systems for Residential Air Conditioning, ACRC CR18, July 1999.

Beaver, A., P. Hrnjak, J. Yin, and C. Bullard, "Effects of Distribution in Headers of Microchannel Evaporators on Transcritical CO2 Heat Pump Performance," Proceedings of the ASME Advanced Energy Systems Division, 2000, Orlando, FL, pp. 55-64.

Elbel, S. and P. Hrnjak, 2004, "Flash Gas Bypass for Improving the Performance of Transcritical R744 Systems that Use Microchannel Evaporators," International Journal of Refrigeration, 27:7, 724-735, 12 pp.

ACKNOWLEDGEMENT

The authors thankfully acknowledge the support provided by the Air Conditioning and Refrigeration Center at the University of Illinois at Urbana-Champaign.